Chemistry–A European Journal

Supporting Information

Structure- and Interaction-Based Design of Anti-SARS-CoV-2 Aptamers

Vladimir Mironov, Irina A. Shchugoreva, Polina V. Artyushenko, Dmitry Morozov, Nicola Borbone, Giorgia Oliviero, Tatiana N. Zamay, Roman V. Moryachkov, Olga S. Kolovskaya, Kirill A. Lukyanenko, Yanling Song, Iuliia A. Merkuleva, Vladimir N. Zabluda, Georgy Peters, Lyudmila S. Koroleva, Dmitry V. Veprintsev, Yury E. Glazyrin, Ekaterina A. Volosnikova, Svetlana V. Belenkaya, Tatiana I. Esina, Anastasiya A. Isaeva, Valentina S. Nesmeyanova, Daniil V. Shanshin, Anna N. Berlina, Nadezhda S. Komova, Valery A. Svetlichnyi, Vladimir N. Silnikov, Dmitriy N. Shcherbakov, Galina S. Zamay, Sergey S. Zamay, Tatyana Smolyarova, Elena P. Tikhonova, Kelvin H.-C. Chen, U-Ser Jeng, Gerolama Condorelli, Vittorio de Franciscis, Gerrit Groenhof, Chaoyong Yang, Alexander A. Moskovsky, Dmitri G. Fedorov, Felix N. Tomilin, Weihong Tan, Yuri Alexeev,* Maxim V. Berezovski,* and Anna S. Kichkailo*

Supplementary Information

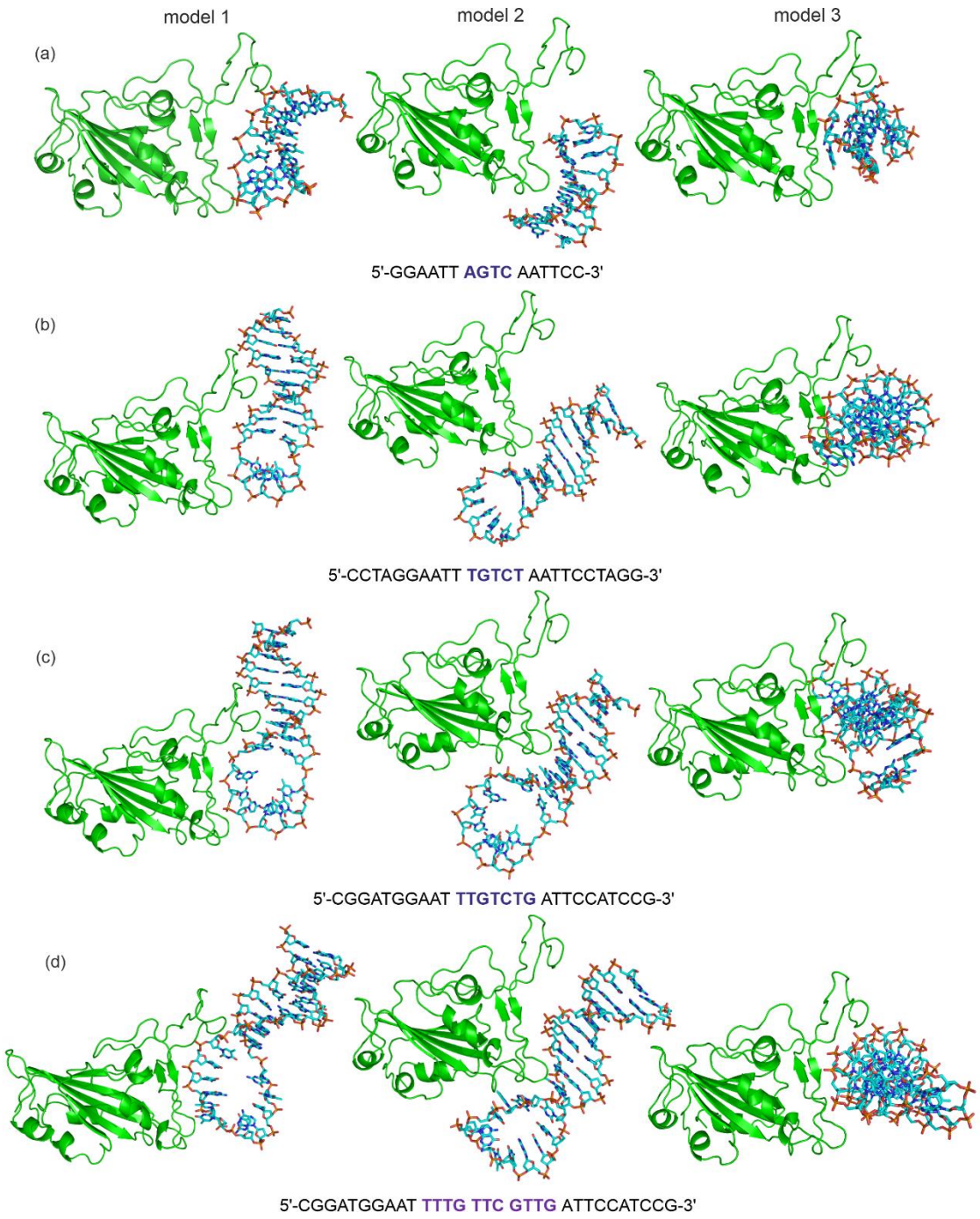

Figure S1. Aptamer/RBD complexes obtained from docking (HDOCK). RBD is in green; aptamer's C atoms are cyan, N atoms are dark blue, O atoms are red, P atoms are orange.

(a) Apt16, (b) Apt25, (c) Apt27, and (d) Apt31.

Table S1. Pairwise hydrogen bonds in RBD/Aptamer complexes. The number in parentheses indicates the conformer number.

RBD/Apt16 (1)		RBD/Apt16 (2)		RBD/Apt25 (1)		RBD/Apt25 (2)	
Residue	Nucleotide	Residue	Nucleotide	Residue	Nucleotide	Residue	Nucleotide
GLU 406	C 16	ARG 454	T 9	ARG 408	T 15	ASP 405	C 14
ARG 408	G 1	ARG 457	T 9	ARG 408	T 10	ARG 408	C 14
ARG 408	G 2	LYS 458	G 8	ARG 408	T 13	ARG 408	T 15
ARG 408	A 3	LYS 458	A 7	GLN 409	T 10	ARG 408	T 13
ARG 408	C 15	LYS 462	G 7	GLN 414	T 10	ARG 408	T 15
ARG 408	C 16	ILE 468	T 9	THR 415	T 10	GLN 409	T 10
GLY 413	G 1	SER 469	T 9	LYS 417	T 11	GLN 414	T 10
GLN 414	G 1	GLU 471	G 8	GLY 504	T 15	THR 415	T 10
GLN 414	G 2	ASN 481	A 4	TYR 505	T 15	LYS 417	T 11
THR 415	C 16			TYR 505	T 13	GLY 504	C 14
LYS 417	C 15			TYR 505	C 14	GLY 504	T 15
ILE 418	C 16					TYR 505	T 15
RBD/Apt27 (1)		RBD/Apt27 (2)		RBD/Apt31 (1)		RBD/Apt31 (2)	
Residue	Nucleotide	Residue	Nucleotide	Residue	Nucleotide	Residue	Nucleotide
ARG 346	G 2	ARG 403	T 14	LEU 368	G 14	THR 376	T 12
ARG 346	G 3	ARG 403	C 15	TYR 369	T 16	PHE 377	T 12
LYS 444	G 3	ARG 403	T 16	TYR 369	G 14	TYR 380	T 11
LYS 444	A 4	LYS 417	T 15	SER 373	G 14	THR 385	T 16
GLY 446	C 21	ASN 448	G 6	PHE 374	G 14	ARG 408	T 24
ASN 448	G 3	ASN 448	G 7	THR 376	T 13	ARG 408	C 25
TYR 449	T 20	ASN 487	T 5	THR 376	T 15	ARG 408	T 10
ASN 450	G 3	ASN 487	A 4	CYS 379	T 16	ARG 408	T 11
SER 494	C 21	PHE 490	G 17	THR 385	T 16	ARG 408	T 24
GLN 498	A 18	GLN 493	T 16	ARG 408	T 24		
GLN 498	T 19	GLN 493	G 17	ARG 408	T 11		
THR 500	T 19	TYR 495	C 15	ARG 408	T 12		
THR 500	A 18	TYR 495	T 16	ARG 408	T 23		
ASN 501	T 19	GLN 498	A 8				
		GLN 498	T 10				
		GLN 498	A 18				
		TYR 505	G 13				

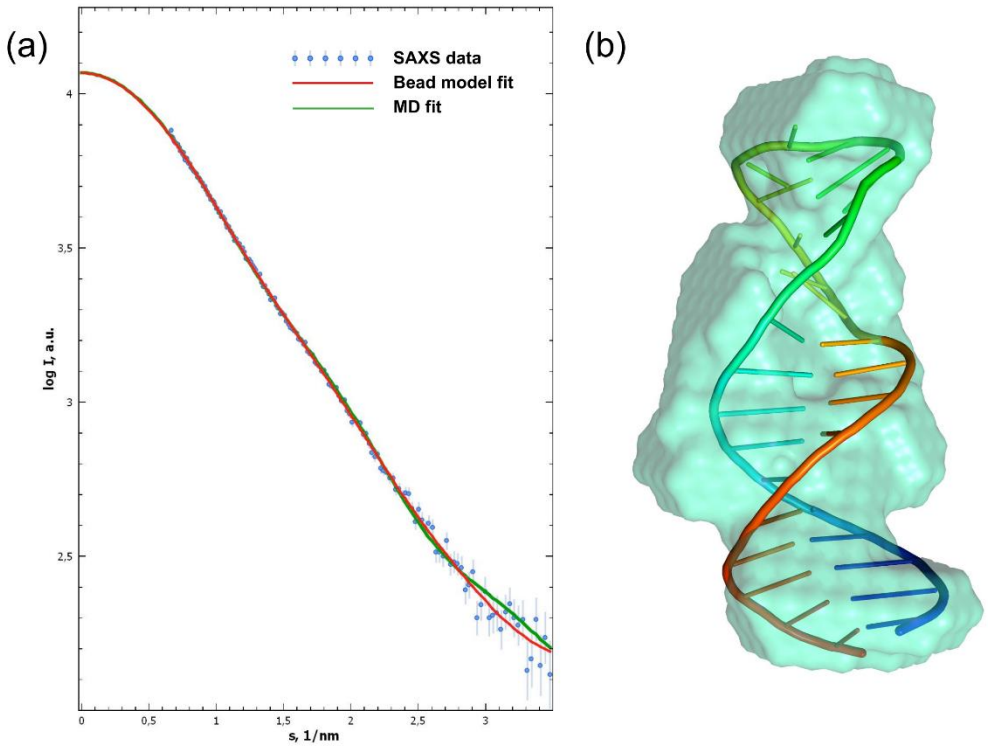

Figure S2. (a) Experimental SAXS data (blue circles with the light blue error bars) fitted by the theoretical SAXS curves calculated from the bead model based on the p(r) (red) and from the MD model (green) of aptamer Apt31. (b) Comparison of the Apt31 MD-structure (colored cartoon) with the SAXS bead model (cyan volume).

Verification of quantum chemistry method used in FMO calculation

In this work, we used the RI-MP2/6-31G(d,p) method for computing interaction energies within the FMO approach. To estimate the impact of the method selection, we computed the pair interaction energy of two most strongly interacting fragments in the RBD-Apt31(1) complex: Arg408 and Thy23 using different methods. The fragments were extracted from the complex and the free valances at the interfragment covalent bonds were saturated with hydrogen atoms. Positions of the capping hydrogens were optimized with the B3LYP/6-31G(d,p) method while keeping all other atoms fixed.

For interaction energy calculation we used the RI-MP2 method (same as in FMO), and DFT with dispersion correction (B3LYP and wB97X-D3 functionals). For DFT we also computed interaction energy with a triple-zeta basis. Also, the BSSE corrections have been estimated using the full dimer basis for calculating energies of each monomer. The results of calculation are presented in Tables S2 and S3. We also present the corresponding values for these two fragment interactions which were extracted from the FMO calculations. Because it is not currently possible to estimate BSSE correction in FMO/MP2 method, the corresponding values are not presented in Table S3. Note that within the FMO approach the RI-MP2 method is faster and typically shows better convergence than the DFT method.

Table S2. Interaction energies of the aminoacid residue and nucleotide system in vacuum. We used Arg408 of SARS-CoV-2 Spike protein RBD and Thy23 of the Apt31 aptamer in the RBD-Apt31(1) complex. The corresponding values from the FMO calculations (with and without PCM) are presented for comparison.

	$E_{Arg+Thy}$, *a.u.*	E_{Arg}, *a.u.*	E_{Thy}, *a.u.*	ΔE_{pair}, *kcal/mol*
RI-MP2/6-31G(d,p) (vac.)	-1893.972917	-530.099598	-1363.713252	-100.44
B3LYP-D3(BJ)/cc-pVDZ (vac.)	-1899.147098	-531.757117	-1367.222322	-105.21
B3LYP-D3(BJ)/cc-pVTZ (vac.)	-1899.713947	-531.933451	-1367.621770	-99.60
wB97X-D3/cc-pVDZ (vac.)	-1898.729045	-531.631799	-1366.929327	-105.37
wB97X-D3/cc-pVTZ (vac.)	-1899.245164	-531.787863	-1367.297088	-100.53
FMO2 (RI-MP2/6-31G(d,p)) (vac.)	-1861.311992	-513.702355	-1347.413010	-123.38
FMO2 (RI-MP2/6-31G(d,p)) (PCM water solvent)	-1861.356758	-513.763602	-1347.426701	-104.45

Table S3. Interaction energies of the aminoacid residue and nucleotide system in vacuum (See Table S2) evaluated in the full basis of dimer. BSSE errors have been estimated using counterpoise correction with respect to the interaction energies presented in Table S2.

	$E_{Arg+Thy}$, a.u.	E_{Arg} (dimer basis) a.u.	$E_{Thy}(dimer\ basis)$ a.u.	$\Delta E_{pair}+BSSE$, kcal/mol	BSSE error, %
RI-MP2/6-31G(d,p) (vac.)	-1893.972917	-530.100440	-1363.720630	-95.28	5.1
B3LYP-D3(BJ)/cc-pVDZ (vac.)	-1899.147098	-531.757585	-1367.232518	-98.51	6.4
B3LYP-D3(BJ)/cc-pVTZ (vac.)	-1899.713947	-531.933690	-1367.624999	-97.42	2.2
wB97X-D3/cc-pVDZ (vac.)	-1898.729045	-531.632203	-1366.938116	-99.60	5.5
wB97X-D3/cc-pVTZ (vac.)	-1899.245164	-531.788056	-1367.299888	-98.66	1.9